Title

Morphological and dynamic contrast enhanced MR imaging features for the differentiation of chordoma and giant cell tumors in the Axial Skeleton

Journal

Journal of Magnetic Resonance Imaging, 45(4)

ISSN

1053-1807

Authors

Lang, Ning
Su, Min-Ying
Xing, Xiaoying
et al.

Publication Date

2017-04-01

DOI

10.1002/jmri.25414

Peer reviewed

Published in final edited form as:

J Magn Reson Imaging. 2017 April ; 45(4): 1068–1075. doi:10.1002/jmri.25414.

Morphological and Dynamic Contrast Enhanced MR Imaging Features for the Differentiation of Chordoma and Giant Cell Tumors in the Axial Skeleton

Ning Lang, MD[1], **Min Ying Su, PhD**[2,*], **Xiaoying Xing, MD**[1], **Hon J. Yu, PhD**[2], and **Huishu Yuan, MD**[1,*]

[1]Department of Radiology, Peking University Third Hospital, Beijing, China

[2]Tu & Yuen Center for Functional Onco-Imaging, Department of Radiological Sciences, University of California, Irvine, California, USA

Abstract

Purpose: To characterize the morphological and dynamic-contrast-enhanced (DCE) MRI features of chordoma and giant cell tumor (GCT) of bone occurring in the axial skeleton.

Materials and Methods: A total of 13 patients with chordoma and 26 patients with GCT who received conventional T1, T2, and DCE-MRI on 3 Tesla MR scanners were retrospectively identified and analyzed. Two radiologists evaluated morphological features independently, including the lesion location, expansile bone changes, vertebral compression, presence of paraspinal soft tissue mass, fibrous septa, and the signal intensity on T1WI and T2WI. The inter-observer agreement was evaluated by kappa test. The DCE kinetics was measured to obtain the initial area under curve (IAUC) and the wash-out slope; also the two-compartmental pharmacokinetic model was applied to obtain K^{trans} and k_{ep}. The diagnostic accuracy was evaluated by CHAID decision tree and ROC analysis.

Results: Chordomas were more likely to show soft tissue mass than GCTs (13/13 = 100% versus 15/26 = 58%; $P = 0.007$), as well as fibrous septa (9/13 = 69% versus 0; $P<0.001$). In decision tree analysis, presence of fibrous septa and lesion location yield 31/39 = 79% accuracy. The DCE-MRI pharmacokinetic parameters K^{trans} and k_{ep} of GCTs were significantly higher than those of chordomas, 0.136 0.65 versus 0.0660.04 (1/min) for K^{trans}, 0.6260.22 versus 0.176 0.12 (1/min) for k_{ep}, $P<0.001$ for both. If using kep = 0.43/min as the cut-off value, it achieved 100% sensitivity and 92% specificity to differentiate chordoma from GCT, with an overall accuracy of 37/39 = 95%. The IAUC was highly correlated with K^{trans} (r = 0.94), and the slope was highly correlated with k_{ep} (r = 0.95).

Conclusion: Several morphological features were significantly different between chordoma and GCT, but their diagnostic performance was inferior to that of DCE-MRI.

*Address reprint requests to: M.-Y.S., 164 Irvine Hall, Center for Functional Onco-Imaging, University of California, Irvine, CA 92697-5020., msu@uci.edu; H.Y., Department of Radiology, Peking University Third Hospital, 49 North Garden Road, Haidian District, Beijing, 100191, PR China. huishuy@bjmu.edu.cn.

Additional Supporting Information may be found in the online version of this article.

Chordoma and giant cell tumor (GCT) in the axial skeleton are primary tumors of bone, with similar clinical symptoms. On imaging, both are characterized with osteolytic bone destruction, lesions of heterogeneous signal intensity, and cystic regions.[1,2] Chordoma was most often present in the clival and sacral regions, and the lesion location was commonly used as the diagnostic indicator.[3] Therefore, when GCT occur in basilar clivus, cervical C1–2 or sacral vertebra, it may be inaccurately diagnosed as chordoma based on the location.[2] In sacrum, chordoma and GCT of bone are the top one and two common primary tumors.[4] Also, as more chordomas were reported to occur in various segments of the spine, misdiagnosing the lesion based on its location can occur.[3,5]

Surgery is the main treatment for chordoma and GCT, however, with different approaches used. Hence, an accurate preoperative diagnosis and staging would be helpful for surgical planning and determining the need for adjuvant therapy. The purpose of this study is to evaluate the morphological features on T1 and T2 weighted images and the parameters analyzed from dynamic contrast enhanced MRI (DCE-MRI) for the differentiation of chordoma and GCT.

Materials and Methods

Patients

Thirty-nine patients were analyzed in this retrospective study. There were a total of 13 chordoma cases (7 males and 6 females; mean age 47 years old), 9 cases occurring in clivus and cervical vertebra and 4 cases occurring in sacrococcyx. There were 26 cases of GCT (16 males and 10 females; mean age 33 years old), 11 cases in cervical vertebra, 7 cases in thoracic vertebra, 6 cases in lumbar vertebra, 2 cases in sacral vertebra. These patients were identified through a search of our clinical MRI database in 2009– 2014, from patients who received an MRI examination including a DCE-MRI sequence. To be eligible for this study, patients should not have received any biopsy, surgery or other treatments before MRI. This study was approved by the Ethics Committee of our hospital, and the informed consent was waived.

MR Imaging Protocol

The studies were performed on a Siemens Trio 3 Tesla (T) MR scanner (2009–2013) and a GE Discovery MR750 3T scanner (2013–2014), using a similar protocol. When changing the scanner from Siemens to GE, one major requirement was to make the image contrast and quality of the GE scanner consistent with those of the Siemens scanner. The conventional imaging sequences included transverse T_2WI, sagittal T_2WI without and with fat suppression, and sagittal T_1WI, acquired by using the fast spin echo pulse sequence. Next the DCE-MRI was performed by injecting Gd-DTPA (0.1 mmol/kg) using the Ulrich power injector at a flow rate of 2 mL/s, followed by 20 mL saline for flushing at the same rate. The DCE sequence on the Siemens scanner was the FLASH three-dimensional (3D) VIBE (volume interpolated breathhold examination), TR = 4.1 ms, TE = 1.5 ms, flip angle = 10°, acquisition matrix = 256 × 192, field of view (FOV) = 250 × 250 mm. A total of 30 slices, 3 mm thick with a gap of 0.6 mm, was prescribed to cover the entire abnormal region. Each dynamic frame was 10–14 s, and 12 frames were acquired with a total DCE time period of

120–168 s. When the study was moved to the GE scanner, a DCE-MRI protocol by using the LAVA (Liver Acceleration Volume Acquisition) pulse sequence with similar spatial and temporal resolution was used.

Image Analysis

The images were evaluated by two radiologists (N.L. and X.X.) independently. They were experienced in diagnosis of spinal diseases with 10 and 7 years of experience, respectively. The segment involved, the presence of expansile bone changes (yes or no), the degree of vertebral compression (>50%, <50%, or no), disruption of bone cortex (yes or no), paraspinal soft tissues mass (yes or no), fibrous septa in T2-weighted soft tissues (yes or no), were tabulated. The signal intensity of the lesion on T1WI and T2WI were evaluated by using the intensity of the spinal cord as the reference, and determine as “low”, “equal”, or “high” when the intensity of the lesion was lower than, equal to, or higher than that of the spinal cord, respectively. On T2WI, because CSF signal was higher than that of the spinal cord, we added one more category as “very high” when the intensity of the lesion was comparable to that of the CSF.

A manual region of interest (ROI) ranging from 0.5 to 1.2 cm^2 was placed in the most overtly enhanced area in the lesion, excluding regions with cystic lesions, calcification, necrosis, and hemorrhage, etc. Two radiologists drew the ROI separately. Siemens Sygno Mean Curve software was used to measure the signal intensity time course of the selected ROI. The semiquantitative and quantitative DCE-MRI analysis methods were applied to characterize spinal tumors.[6,7] Based on the signal intensity time course the DCE kinetic pattern was separated into three categories: (1) the wash-out pattern: reaching the peak near 1-min and showing wash-out with >10% slope from the peak; (2) the plateau pattern: the signal intensity remaining at a constant level after 1-min with less than 10% change; (3) the persistent enhancement pattern: the signal intensity continuing to increase in the DCE period with > 10% change from the intensity at 1-min.

The temporal resolution varied slightly, so the data points in the DCE period were not exactly the same for all cases. For cases that had a peak value in the DCE period, the peak most often occurred around the 67-s time point. The initial area under curve (IAUC) was measured by averaging the signal enhancements of data points after injection to the 67-s time point or the closest time point after 67 s. The wash-out slope was calculated based on the peak intensity and the signal intensity at the last time point, as: $[(S_{last}\text{-}S_{peak})/S_{peak} \times 100\%]$; or if there was no peak, the signal intensity around 67 s was used as the reference $[(S_{last}\text{-}S_{67s})/S_{67s} \times 100\%]$. The enhancement kinetics was also analyzed by using the two-compartmental Tofts model containing vascular and interstitial spaces, with the in-flux transport rate from vascular to interstitial space as K^{trans}, and the out-flux transport rate from interstitial to vascular space as k_{ep}.[8,9] The fast population-averaged blood curve by Parker et al[10] was used as the reference (same as the parameters used in Siemens syngo Tissue 4D software). In the analysis, the vascular contribution (that is, the vascular volume) was ignored, and only two parameters K^{trans} and k_{ep} were used in the fitting.

Statistical Analysis

The inter-observer agreement between the morphological parameters read by two radiologists were assessed by using the kappa test, and the DCE parameters analyzed from the ROI drawn by two radiologists were compared using the Pearson's correlation. The χ^2 Test was used to compare the incidence segments, the degree of vertebral compression, whether there was expansile bone changes, disruption of bone cortex, presence of paraspinal soft tissues mass, fibrous septa in T2 soft tissue, as well as the signal intensity of the lesion seen on T1WI and T2WI. The test was also applied to compare the differences in the DCE kinetic patterns of chordoma and GCT. Pearson's correlation was used to correlate the heuristic DCE-MRI parameters (IAUC and slope) and the pharmacokinetic parameters (K^{trans} and k_{ep}). The results obtained by the more senior radiologist were used for the final statistical analysis. The CHAID (CHi-squared Automatic Interaction Detection) decision tree was used to analyze the diagnostic performance of personal factors (age and sex) and morphological parameters to differentiate between chordoma and GCT. Software SPSS version 18 was used, and $P<0.05$ indicated a significant difference. The receiver operating characteristic (ROC) analysis was performed to evaluate the performance of DCE-MRI heuristic and pharmacokinetic parameters to differentiate between chordoma and GCT, by using MedCalc (Mariakerke, Belgium).

Results

Morphological Imaging Features

The results are summarized in Table 1. The lesion location segment was categorized into Clivus and C1, C2 (because lesions in this region could not be clearly separated), cervical C3–C7, thoracic, lumbar, and sacral regions. Chordomas mainly occurred in the Clivus, C1, C2 and Sacrales (12/13 = 92%), and GCTs were seen in all segments. GCTs were more likely to show vertebral compression (14/26 = 54%) than chordomas (3/10 = 30%), but not reaching the significance level. Almost all lesions showed disruption of bone cortex. All chordomas had soft tissue masses and 9/13 (69%) showed fibrous septa. In contrast, only half GCTs (15/26 = 58%) had soft tissue mass and none showed fibrous septa. Figure 1 shows one chordoma and one GCT that demonstrate these typical morphological features.

The CHAID decision tree diagnostic test found that the presence of fibrous septa in T2 soft tissues and the lesion location segment were diagnostic markers. When fibrous septa was present, all 9 cases were chordomas. In the remaining 30 cases without fibrous septa, when the lesion occurring in cervical, thoracic, and lumbar segments, all 22 cases were GCTs. Combining these two markers would yield 31/39 = 79% accuracy. For the eight cases that were not correctly diagnosed, four were chordomas (three in C2, one in S3–5) and four were GCTs (two in C2, one in S1, one in S2). For the signal intensity on T2WI with and without fat suppression, there were significant differences between chordoma and GCT and could help in making diagnosis, but they were not selected in the CHAID diagnostic model.

DCE Kinetic Patterns

All lesions showed strong contrast enhancements. In DCE kinetic patterns, 16 of 26 GCT cases showed the wash-out pattern, 8 had the plateau pattern, and 2 showed the persistent

enhancement pattern. Figure 2 shows one GCT with the wash-out DCE pattern, and Figure 3 shows another GCT case with the plateau DCE pattern. In contrast, no chordoma showed the wash-out pattern, 3 showed the plateau, and most of them (10/13) showed the persistent enhancement pattern. Figures 4 and 5 show two chordoma patients demonstrating the persistent enhancement DCE pattern. The difference in the DCE patterns of GCT and chordoma was highly significant ($P< 0.001$).

Quantitative DCE Parameters

Pharmacokinetic parameters analyzed using the twocompartmental model also showed a highly significant difference. The K^{trans} of GCT was higher than that of chordoma (0.13 ± 0.65 versus 0.06 ± 60.041; $P< 0.001$). The k_{ep} of GCT was also higher than that of chordoma (0.62 ± 0.22 versus 0.17 ± 0.12/min; $P<0.001$). The ROC analysis was performed to evaluate the diagnostic performance, and the area under the curve (AUC) was 0.845 (95% confidence interval [CI]: 0.705–0.984) for K^{trans} and 0.963 (95% confidence interval 0.908–1.000) for k_{ep}. When using k_{ep} 50.43/min as the cutoff value, it achieved 100% sensitivity and 92% specificity to differentiate chordoma from giant cell tumor, with an overall accuracy of (37/39 = 95%). The distribution of k_{ep} for GCT and chordoma is shown in Figure 6. Figure 7 shows the correlation between IAUC and K^{trans} (r = 0.94), and between wash-out slope and k_{ep} (r = 0.95). The heuristic parameters analyzed directly from the DCE time course were highly correlated with pharmacokinetic parameters. In ROC analysis, the AUC was 0.849 (95% CI: 0.710–0.988) for IAUC, and 0.973 (95% CI: 0.930–1.000) for wash-out slope. The heuristic and pharmacokinetic parameters were highly correlated, and their diagnostic performances were almost identical.

Inter-observer Agreement

The morphological parameters read by two radiologists independently showed a high degree of agreement, with kappa ranging from 0.835 to 1.0 (complete agreement). The worst agreement was for the determination of expansile bone changes (kappa 50.835), and the values for all other parameters were higher than 0.916. The DCE kinetics analyzed from the ROI drawn separately by the two radiologists also showed a high consistency, with Pearson's correlation r >0.95 for all four analyzed DCE parameters.

Discussion

Chordoma is a rare bone tumor originating in residual embryonic notochord. It accounts for approximately 1–4% of primary bone tumors, and most commonly occurring in the spheno-occipital (clivus) and sacrococcygeal regions.[3] However, there are reports indicating increased incidence in other mobile segments of the spine.[3,5] Boriani et al reported a large series of 52 cases of spinal chordoma that were collected over 50 years, and among them 29% were in cervical vertebrae, 13% in thoracic vertebrae, and 58% in lumbar vertebrae.[5]

Giant cell tumor can affect any bone, most commonly the long bones but can also be seen in the vertebra and sacrum.[11] GCTs in the long bones have distinct imaging features[11–13] in contrast, those occurring in the axial skeleton present with more atypical features.[14] Both

chordomas and GCTs in the spine can compress nerve root or spinal cord, and cause pain, weakness, or even paraplegia.[15]

Because these two lesions in the spine are rare, there are few systematic studies to report their MR imaging features in the literature. In this study we evaluated several specific morphological imaging features. Chordoma can easily break the cortex of bone and form mushroom-shaped soft tissue masses in paraspine or outside dura mater. In our study, all chordomas and only approximately half GCTs had soft tissue mass. Chordomas are slow growing tumors. Fluid and gelatinous mucoid substance (associated with recent and old hemorrhage), necrotic areas, and fibrosis are common; also physaliphorous cells are classically seen on microscopy.[16] On MRI, these features might present as fibrous septa in chordoma, as well as the high signals on fat-suppressed and non–fat-suppressed T2WI.[17,18]

In contrast, the GCT was more likely to show vertebral compression compared with chordoma.[19] As shown in the table, the lesion location segment, fibrous septa, paraspinal soft tissue mass, and the signal intensity in fat-sat and non–fat-sat T2WI showed significant differences between chordoma and GCT. When applying the CHAID decision tree analysis to evaluate their diagnostic performance, only two parameters, fibrous septa and lesion location segment, were selected in the model, but the accuracy was only 79%.

In the interobserver agreement analysis, it was found that expansile bone changes had the worst kappa value. The first radiologist found it to be significantly different between GCT and chordoma, but the second radiologist found it to be nonsignificant. When expansile bone changes coexisting with bone compression, it became very difficult to evaluate this feature, thus it was not a reliable diagnostic marker. The agreement for all other analyzed morphological parameters was very good.

In this study, we also applied DCE-MRI to investigate the differences between their vascular properties. DCE-MRI is a standard method used for diagnosis of breast cancer and prostate cancer.[20,21] The signal intensity time course from the tissue contained in the ROI was measured, and that could be analyzed to obtain heuristic parameters (maximum enhancement, wash-in slope, wash-out slope, initial area under curve, etc.) or the pharmacokinetic parameters K^{trans} and k_{ep}; as well as for classification of the DCE kinetics into “wash-out,” “plateau,” or “persistent enhancement” pattern.[6,7]

The DCE kinetic pattern was significantly different between GCT and chordoma. Consistent with a much higher proportion of GCT cases showed the early peak enhancement with the wash-out DCE pattern, the obtained pharmacokinetic parameters K^{trans} and k_{ep} were also much higher in GCT than in chordoma. When using k_{ep} = 0.43/min as the cut-off value, it could reach 95% accuracy. We also calculated the heuristic parameters that could be easily measured from the DCE time course, and showed a high correlation between IAUC and K^{trans}, and between wash-out slope and k_{ep}. In ROC analysis the diagnostic performances of heuristic and pharmacokinetic parameters were almost identical. For pharmacokinetic model analysis, the optimal method required the measurement of T1 (that is T1-mapping) and the measurement of the precontrast T10 value, so the change of T1 that was proportional to the (Gd) concentration could be measured and used in the analysis.

Because we used the signal intensity time course, not the change of T1, in the two-compartmental model fitting, we were interested in investigating how the obtained parameters K^{trans} and k_{ep} were correlated with heuristic parameters (IAUC and wash-out slope) directly calculated from the DCE kinetics. The IAUC was averaged from the signal intensities of several data points after contrast injection, which was the most robust parameter to show how fast the signal increased during the initial rise phase. For the delayed phase, evaluation of the DCE kinetic pattern using washout, plateau, and persistent enhancement was very common; unfortunately, it did not give a quantitative value that could be used for statistical analysis. Therefore, we tried to come up with a method that could yield the value of the slope in a standardized way. The high correlation between K^{trans} and IAUC, and between k_{ep} and wash-out slope, showed that these parameters could be used as the quantitative characteristic features of the DCE kinetics during the initial phase and the delayed phase as diagnostic markers.

GCT is a benign but very aggressive disease, with a rich blood supply and can present local invasion and further lung metastasis.[22] GCT contains over-proliferation of osteoclasts and numerous thin walled vascular channels predisposing to areas of hemorrhage and presumably related to the common co-existence of cystic regions.[11,23–25] Microscopic observation also demonstrates a high microvessel density, and most microvascular structure is incomplete with irregular lumen, thin lumen wall, disorderly arranged, loss of endothelial cells in some vessel walls, and these will present as leaky vessels that have a high vascular permeability. These vascular properties are consistent with a high angiogenesis that will allow a rapid delivery of Gd-DTPA into the tumor to show a strong enhancement and then followed by a rapid wash-out. In contrast, although chordoma is malignant, but slow-growing without overt angiogenesis.[18] The tumor usually contains abundant myxoid stroma and the secreted mucus arranges as nest or strip as teardrop cells, and they may retain the MR contrast agents and make them difficult to be cleared. Combined with the lack of a rich blood supply, the DCE kinetics of chordoma was very likely to show the persistent enhancement pattern. Therefore, based on their different vascular/cellular properties, DCE-MRI could reach a high accuracy to make differential diagnosis.

We have tried to investigate the added value of the combined morphological and DCE parameters in making differential diagnosis. When performing separate analysis, the CHAID decision tree found fibrous septa and lesion location segment as two morphological diagnostic markers, but the accuracy was inferior to that of DCE parameters. Although CHAID is preferred for categorical parameters, we combined K^{trans} and k_{ep} (using binning strategy) with the morphological parameters and performed the CHAID decision tree analysis. In the combined analysis, k_{ep} was the only selected diagnostic marker to reach 95% accuracy by itself, and none of the morphological parameters could add any value. Furthermore, due to the different nature of categorical and continuous variables, it was difficult to build a combined diagnostic model.

This study has several limitations. The major one was the analysis of K^{trans} and k_{ep} using the signal intensity not the change of T1, also not based on individually measured arterial input function; therefore, the obtained cut-off value may not be applicable to other studies. Another limitation was the small population and lack of diversity. For example, most

chordomas were in Clivus, C1, C2, and Sacrales, only one in the cervical region, so we were not able to evaluate the diagnostic accuracy of the atypical lesions. For heuristic DCE parameters, they were directly calculated from the measured signal intensity thus the values might be heavily dependent on the imaging protocols and the intensity profile of the coil, and the results were not generalizable either. Nonetheless, for a single institution, when a large number of cases are collected, they can be used to build a database, and the clinicians or researchers can choose a preferred pharmacokinetic or heuristic analysis method to obtain reliable DCE parameters to aid in diagnosis.

In conclusion, we have shown that some morphological features, including lesion location segment, fibrous septa, paraspinal soft tissue mass, and the signal intensity in fat-sat and non–fat-sat T2WI, could be used to differentiate between chordoma and GCT of bone; but notably their DCE-MRI properties were distinctively different and that could be used to make differential diagnosis with a high accuracy.

Acknowledgments

Contract grant sponsor: NIH/NCI; contract grant number: R01 CA127927; contract grant number: P30 CA62203; Contract grant sponsor: the National Natural Science Foundation of China; contract grant number: 81471634; Contract grant sponsor: the Beijing Natural Science Foundation; contract grant number: 7164309.

References

1. Gerber S, Ollivier L, Lecle`re J, et al. Imaging of sacral tumours. Skeletal Radiol 2008;37:277–289. [PubMed: 18034341]
2. Si MJ, Wang CS, Ding XY, et al. Differentiation of primary chordoma, giant cell tumor and schwannoma of the sacrum by CT and MRI. Eur J Radiol 2013;82:2309–2315. [PubMed: 24035342]
3. Smolders D, Wang X, Drevelengas A, Vanhoenacker F, De Schepper AM. Value of MRI in the diagnosis of non-clival, non-sacral chordoma. Skeletal Radiol 2003;32:343–350. [PubMed: 12719927]
4. Aoki J, Tanikawa H, Ishii K, et al. MR findings indicative of hemosiderin in giant-cell tumor of bone: frequency, cause, and diagnostic significance. AJR Am J Roentgenol 1996;166:145–148. [PubMed: 8571864]
5. Boriani S, Bandiera S, Biagini R, et al. Chordoma of the mobile spine: fifty years of experience. Spine 2006;31:493–503. [PubMed: 16481964]
6. Lang N, Su MY, Yu HJ, et al. Differentiation of myeloma and metastatic cancer in the spine using dynamic contrast enhanced MRI. Magn Reson Imaging 2013;31:1285–1291. [PubMed: 23290477]
7. Lang N, Su MY, Yu HJ, et al. Differentiation of tuberculosis and metastatic cancer in the spine using dynamic contrast-enhanced MRI. Eur Spine J 2015;24:1729–1737. [PubMed: 25749725]
8. Tofts PS, Kermode AG. Measurement of the blood–brain barrier permeability and leakage space using dynamic MR imaging. 1. Fundamental concepts. Magn Reson Med 1991;17:357–367. [PubMed: 2062210]
9. Tofts PS. Modeling tracer kinetics in dynamic Gd-DTPA MR imaging. J Magn Reson Imaging 1997;7:91–101. [PubMed: 9039598]
10. Parker GJ, Roberts C, Macdonald A, et al. Experimentally-derived functional form for a population-averaged high-temporal-resolution arterial input function for dynamic contrast-enhanced MRI. Magn Reson Med 2006;56:993–1000. [PubMed: 17036301]
11. Murphey MD, Nomikos GC, Flemming DJ, et al. From the archives of AFIP. Imaging of giant cell tumor and giant cell reparative granuloma of bone: radiologic-pathologic correlation. Radiographics 2001;21: 1283–1309. [PubMed: 11553835]

12. Chakarun C, Forrester D, Gottsegen C, et al. Giant cell tumor of bone: review, mimics, and new developments in treatment. Radiographics 2013;33:197–211. [PubMed: 23322837]
13. Pereira HM, Marchiori E, Severo A. Magnetic resonance imaging aspects of giant-cell tumours of bone. J Med Imaging Radiat Oncol 2014;58:674–678. [PubMed: 25256094]
14. Hunter CL, Pacione D, Hornyak M, Murali R. Giant-cell tumors of the cervical spine: case report. Neurosurgery 2006;59:E1142–E1143. [PubMed: 17143206]
15. Samartzis D, Foster WC, Padgett D, et al. Giant cell tumor of the lumbar spine: operative management via spondylectomy and shortsegment, 3-column reconstruction with pedicle recreation. Surg Neurol 2008;69:138–141. [PubMed: 17586008]
16. O'Connell JX, Renard LG, Liebsch NJ, Efird JT, Munzenrider JE, Rosenberg AE. Base of skull chordoma. A correlative study of histologic and clinical features of 62 cases. Cancer 1994;74:2261–2267. [PubMed: 7922977]
17. Wippold FJ, Koeler KK, Smirniotopoulos JG. Clinical and imaging features of cervical chordoma. AJR Am J Roentgenol 1999;172:1423–1426. [PubMed: 10227531]
18. Naka T, Boltze C, Kuester D, et al. Intralesional fibrous septum in chordoma: a clinicopathologic and immunohistochemical study of 122 lesions. Am J Clin Pathol 2005;124:288–294. [PubMed: 16040302]
19. Kwon JW, Chung HW, Cho EY, et al. MRI findings of giant cell tumors of the spine. AJR Am J Roentgenol 2007;189:246–250. [PubMed: 17579178]
20. Kuhl CK, Schild HH, Morakkabati N. Dynamic bilateral contrastenhanced MR imaging of the breast: trade-off between spatial and temporal resolution. Radiology 2005;236:789–800. [PubMed: 16118161]
21. Buckley D, Roberts C, Parker G, et al. Prostate cancer: evaluation of vascular characteristics with dynamic contrast-enhanced T1-weighted MR imaging-initial experience. Radiology 2004;233:709–715. [PubMed: 15498903]
22. Fu S, Bai R, Zhao Z, et al. Overexpression of hypoxia-inducible factor1α and vascular endothelial growth factor in sacral giant cell tumors and the correlation with tumor microvessel density. Exp Ther Med 2014;8:1453–1458. [PubMed: 25289039]
23. Meyers SP. MRI of bone and soft tissue tumors and tumorlike lesions, differential diagnosis and atlas. New York: Thieme Publishing Group; 2008.
24. Si MJ, Wang CG, Wang CS, et al. Giant cell tumours of the mobile spine: characteristic imaging features and differential diagnosis. Radiol Med 2014;119:681–693. [PubMed: 24531890]
25. Shi LS, Li YQ, Wu WJ, Zhang ZK, Gao F, Latif M. Imaging appearance of giant cell tumour of the spine above the sacrum. Br J Radiol 2015; 88:20140566. [PubMed: 25923147]

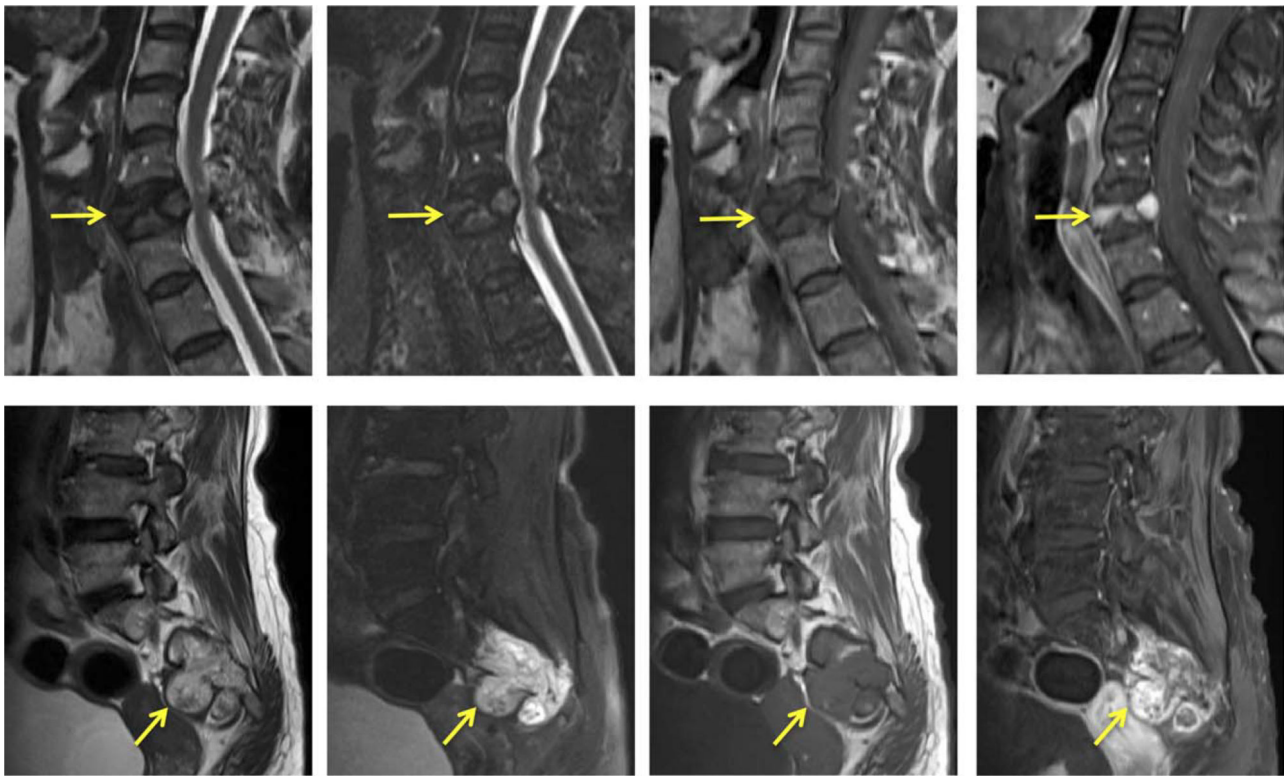

FIGURE 1:
(Top panel) A 63-year-old female with pathologically confirmed GCT of bone. From left to right: T2WI, T2WI with fat suppression, T1WI, and postcontrast T1WI. An osteolytic bone destruction is seen in C6 vertebral body, with vertebral compression more than 50% and visible disruption of bone cortex, but without soft tissue mass. (Bottom panel) A 62-year-old female with pathologically confirmed chordoma. A mixed signal paraspinal soft tissue mass on the right side of S2–3 vertebral body is seen with visible fibrous septa, without vertebral compression.

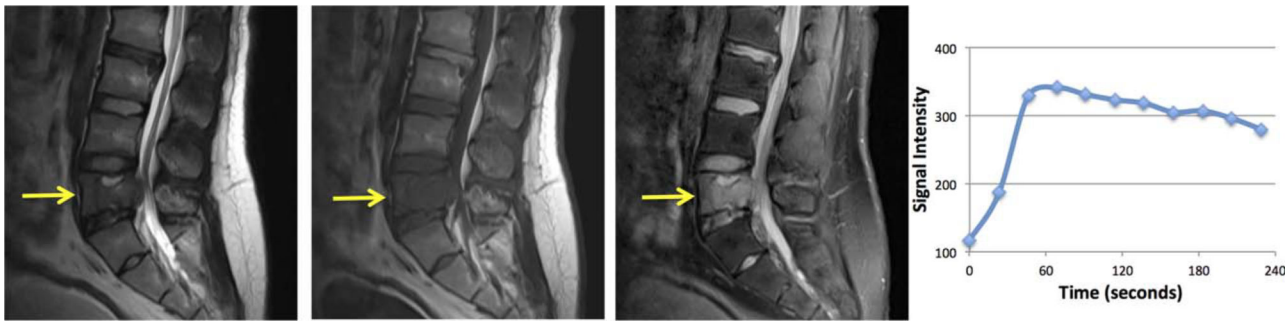

FIGURE 2:

A 21-year-old male with pathologically confirmed GCT of bone. From left to right: T2WI, T1WI, postcontrast T1WI, and signal intensity time course. Bone destruction and vertebral compression is seen in L5 vertebral body, intruding into the spinal canal. A heterogeneously enhanced lesion is seen on postcontrast T1WI. The signal intensity time course shows a clear wash-out pattern with K^{trans} = 0.09/min, k_{ep} = 0.54/min.

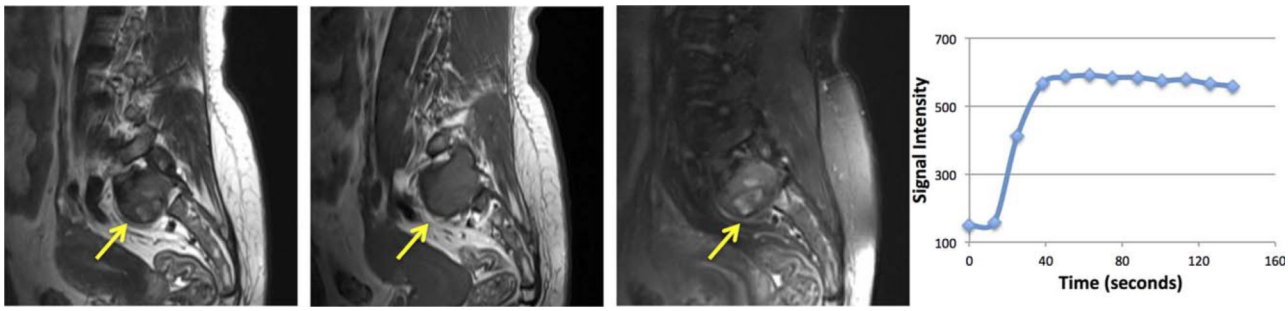

FIGURE 3:

A 45-year-old female with pathologically confirmed GCT of bone. From left to right: T2WI, T1WI, postcontrast T1WI, and signal intensity time course. A mixed signal soft tissue mass is seen on the right side of S1 vertebral body. A heterogeneously enhanced lesion is seen on postcontrast T1WI. The signal intensity time course shows a plateau pattern with K^{trans} = 0.14/min, k_{ep} = 0.46/min.

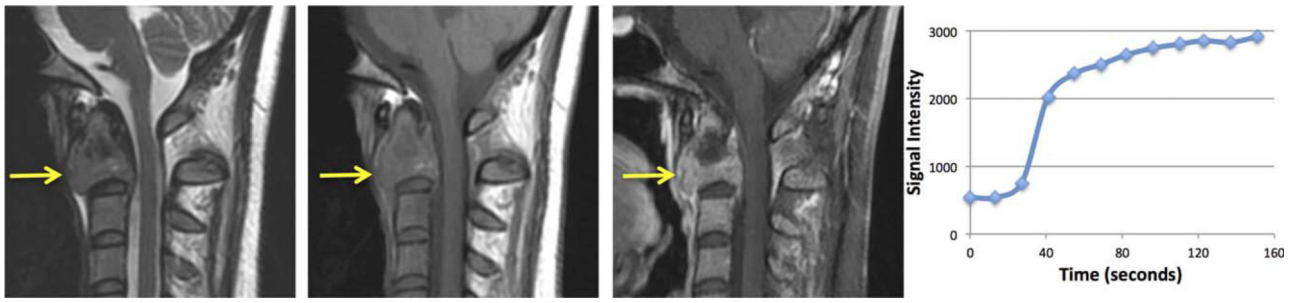

FIGURE 4:

A 22-year-old female with pathologically confirmed chordoma. From left to right: T2WI, T1WI, postcontrast T1WI, and signal intensity time course. A lesion with osteolytic bone destruction is seen in C2 vertebrae showing a mild compression of vertebral body. It presents as a mixed signal soft tissue mass intruding into dural sac and spinal cord. The lesion shows a heterogeneous enhancement on postcontrast T1W1. The signal intensity time course shows a clear persistent enhancement pattern with K^{trans} = 0.15/min, k_{ep} = 0.18/min.

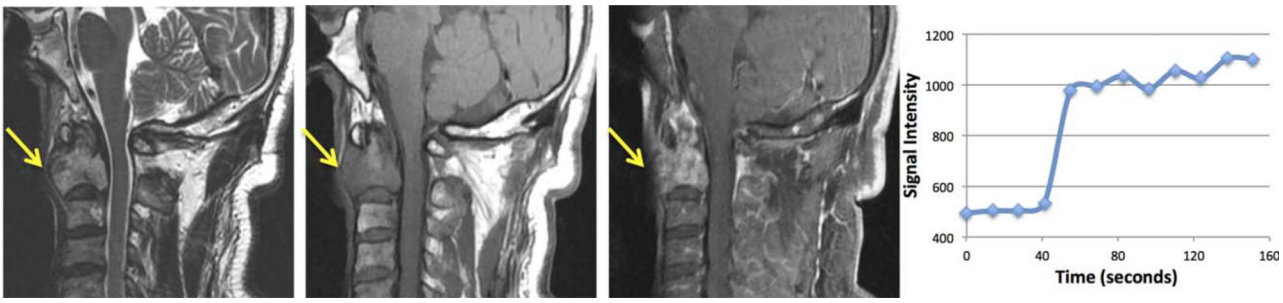

FIGURE 5:

A 53-year-old male with pathologically confirmed chordoma. From left to right: T2WI, T1WI, postcontrast T1WI, and signal intensity time course. A visible lesion with osteolytic bone destruction is seen in C2 vertebral body, showing a mixed signal soft tissue mass intruding into dural sac and spinal cord, without vertebral compression. A heterogeneously enhanced lesion is seen on postcontrast T1WI. The signal intensity time course shows a persistent enhancement pattern with K^{trans} = 0.04/min, k_{ep} = 0.29/min.

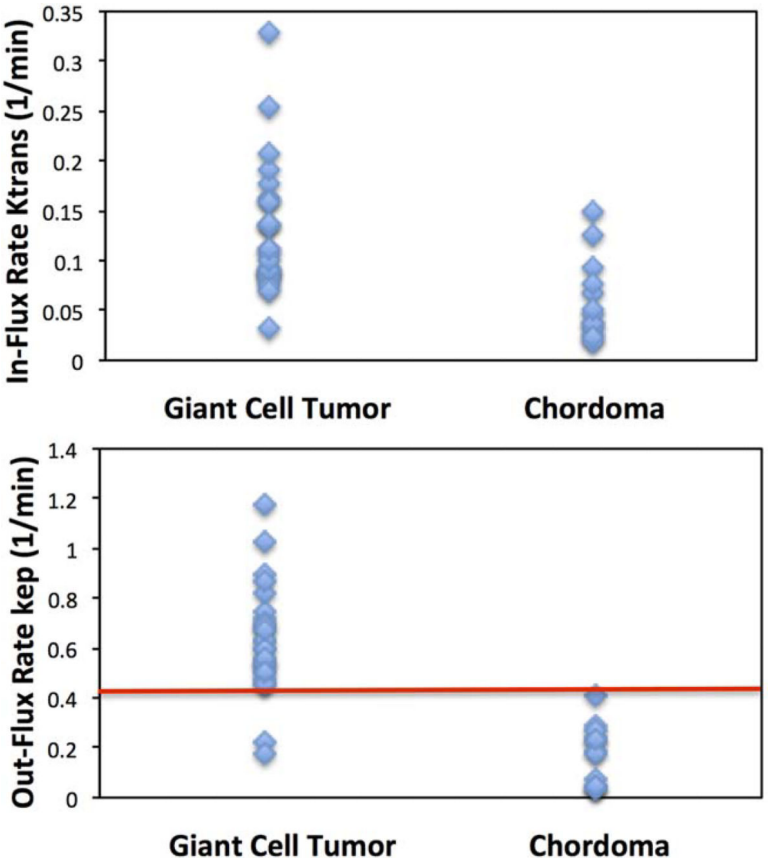

FIGURE 6:

The distribution of K^{trans} and k_{ep} in the GCT of bone and the chordoma groups. The DCE pattern of GCT is more likely to present rapid wash-in followed by wash-out, and it has significantly higher mean K^{trans} and k_{ep} values compared with chordoma. Using k_{ep} = 0.43/min as the cut-off value can achieve a high diagnostic accuracy of 95%.

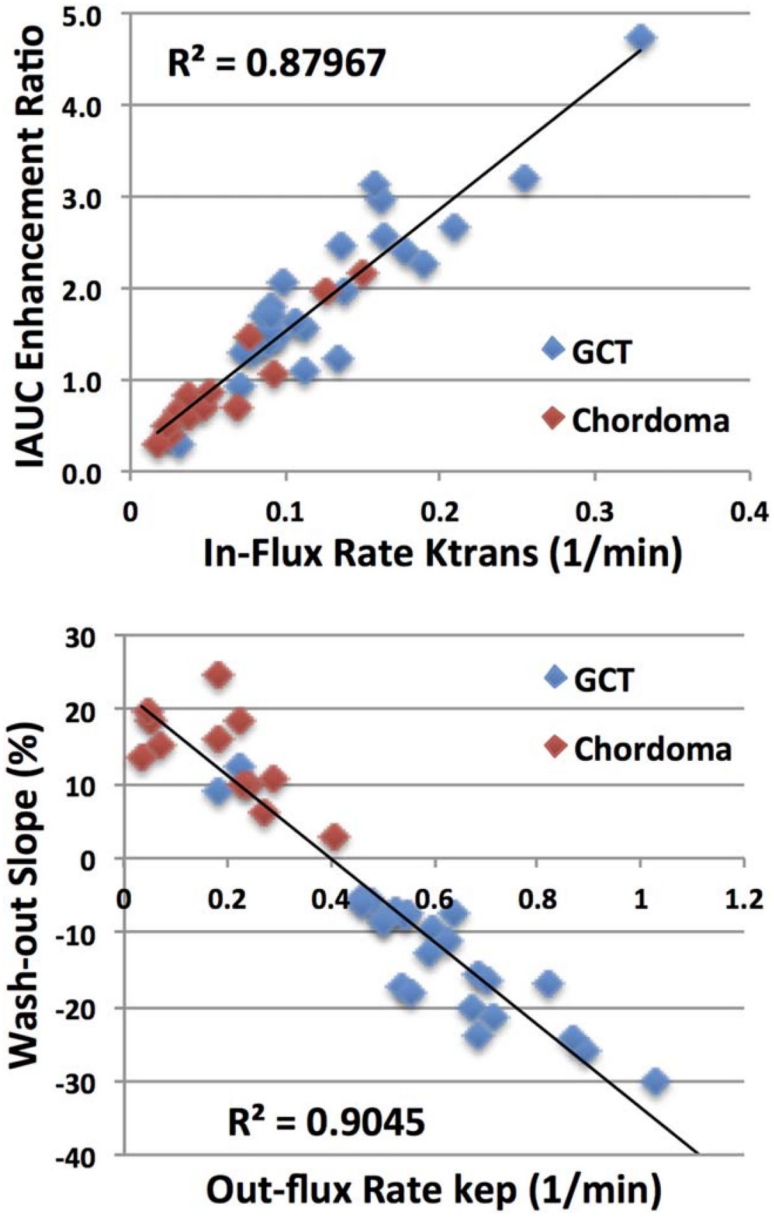

FIGURE 7:

The correlation between heuristic and pharmacokinetic parameters analyzed from DCE-MRI time course. The top figure shows the correlation between the initial area under curve (IAUC) and the in-flux transport rate K^{trans}, with a high coefficient of r = 0.94. The bottom figure shows the correlation between the wash-out slope and the out-flux transport rate k_{ep}, with a high coefficient of r = 0.95.

Table 1.

Comparison of Imaging Features of Chordoma and Giant Cell Tumor of Bone on MRI

		26 Giant cell tumor (%)	13 Chordoma (%)	*P*-Value
Incidence segment	Clivus, C1, C2	2 (7%)	8 (61%)	<0.001
	Cervicales C3-C7	9 (35%)	1(8%)	
	Thoracalis	7 (27%)	0	
	Lumbalis	6 (23%)	0	
	Sacrales	2 (8%)	4 (31%)	
Expansile bone changes	Yes	21 (81%)	4 (31%)	0.004
	No	5 (19%)	9 (69%)	
Vertebral compression	No	12 (46%)	10 (77%)	0.040
	< 50%	8 (31%)	3 (23%)	
	> 50%	6 (23%)	0	
Disruption of bone cortex	Yes	25 (96%)	13 (100%)	1.000
	No	1 (4%)	0	
Paraspinal soft tissue mass	Yes	15 (58%)	13 (100%)	0.007
	No	11 (42%)	0	
Presence of fibrous septa in T2 soft tissues	Yes	0	9 (69%)	< 0.001
	No	26 (100%)	4 (31%)	
T1 solid component signal	Low	1 (4%)	0	1.000
	Equal	25 (96%)	13 (100%)	
	High	0	0	
T2 solid component signal on non-fat-suppressed sequence	Low	0	0	< 0.001
	Equal	20 (77%)	1 (8%)	
	High	4 (15%)	4 (31%)	
	Very High	2 (8%)	8 (61%)	
T2 solid component signal on fat-suppressed sequence	Low	0	0	< 0.001
	Equal	6 (23%)	0	
	High	17 (65%)	2 (15%)	
	Very High	3 (12%)	11 (85%)	
DCE kinetic pattern	Wash-out	16 (61%)	0	< 0.001
	Plateau	8 (31%)	3 (23%)	
	Persistent	2 (8%)	10 (77%)	